Gas Phase Reactions between Acetylene Radical Cation and Water. Energies, Structures and Formation Mechanism of C 2 H 3 O + and C 2 H 4 O +• Ions

ARTICLE *in* THE JOURNAL OF PHYSICAL CHEMISTRY A · AUGUST 2008

Impact Factor: 2.69 · DOI: 10.1021/jp802086z · Source: PubMed

5 AUTHORS, INCLUDING:

Enli Xie
Virginia Commonwealth University
4 PUBLICATIONS **43** CITATIONS
SEE PROFILE

Samuel Abrash
University of Richmond
24 PUBLICATIONS **217** CITATIONS
SEE PROFILE

Michael Noah Mautner
Virginia Commonwealth University
202 PUBLICATIONS **5,193** CITATIONS
SEE PROFILE

M. Samy El-Shall
Virginia Commonwealth University
272 PUBLICATIONS **4,575** CITATIONS
SEE PROFILE

Gas Phase Reactions between Acetylene Radical Cation and Water. Energies, Structures and Formation Mechanism of $C_2H_3O^+$ and $C_2H_4O^{+\bullet}$ Ions

Paul O. Momoh, Enli Xie, Samuel A. Abrash,† Michael Meot-Ner (Mautner), and M. Samy El-Shall*

Department of Chemistry, Virginia Commonwealth University, Richmond, Virginia 23284-2006

Received: March 10, 2008; Revised Manuscript Received: April 14, 2008

Reactions of the acetylene radical cation ($C_2H_2^{+\bullet}$) with H_2O were investigated using ion mobility mass spectrometry. The primary products are the $C_2H_3O^+$ and $C_2H_4O^{+\bullet}$ ions, produced with an overall rate coefficient $k(300\ K) = 2(\pm 0.6) \times 10^{-11}\ cm^3\ s^{-1}$ that increases with decreasing temperature. The $C_2H_4O^{+\bullet}$ (adduct) vs $C_2H_3O^+$ (H loss) ratio also increases with decreasing temperature, and with increasing third-body pressure. Ab initio calculations on the products showed seven stable $C_2H_3O^+$ isomers and eleven stable $C_2H_4O^{+\bullet}$ isomers. In the $C_2H_4O^{+\bullet}$ adduct channel, the reactivity and energetics suggest that the adduct is the $H_2C{=}CHOH^{+\bullet}$ (vinyl alcohol) ion. In the $C_2H_3O^+$ channel, the H loss occurs exclusively from water. The $C_2H_3O^+$ product ion undergoes slow deprotonation by water to form $H^+(H_2O)_n$ clusters. The reactivity, combined with energetics, suggests that the protonated ketene CH_2COH^+ is the most likely observed $C_2H_3O^+$ ion probably with some contribution from the cyclic *c*-CH_2CHO^+ ion.

I. Introduction

Well over one hundred molecules, including acetylene and water are present in interstellar clouds, molecular clouds, solar nebulae, and envelopes expelled by evolved stars.[1–11] Acetylene molecules and ions are also likely to be present in the hydrocarbon-containing ionospheres of Jovian planets, Titan, and in interstellar clouds.[12] Reactions of the linear, branched, and cyclic acetylene ions with water can provide the early steps in the formation processes leading to prebiotic molecules.[9] In interstellar clouds, possible adducts of acetylene and water such as CH_2CHOH and *c*-C_2H_4O were observed, and these molecules could lead to the formation of some of the complex molecular species observed in interstellar medium.[13] These molecules participate in gas phase chemistry, especially ion−molecule reactions. Ionic reactions of acetylene and water can also occur in flames, in industrial polymerization, and in combustion processes where they can contribute significantly to the mechanisms of soot formation.[14]

Gases in solar nebulae are subjected to ionizing radiation and, unlike interstellar clouds, the relatively high gas densities in parts of the nebula can allow three-body processes that form synthetic adducts and clusters.[7,8] The radiation and the high velocity winds break up the carbonaceous compounds in the dust and trigger new reactions including polymerization of ionized acetylene that can lead to the formation of benzene and larger polycyclic aromatic hydrocarbons.[2,4,6] In recent work, we reported evidence for the formation of benzene ions within gas phase ionized acetylene clusters.[15,16] The results from the mass-selected ion mobility and collisional induced dissociation experiments coupled with theoretical calculations indicate that benzene ions are efficiently produced following the ionization of neutral acetylene clusters. Consequently, the ionized acetylene trimer and the benzene cation exhibit similar stepwise association and size-dependent proton transfer reactions with water molecules.[16] On the other hand, ion-molecule reactions between the acetylene radical cation ($C_2H_2^{+\bullet}$) and water have not been investigated. Only the reactions of H_3O^+ with C_2H_2 under radiative and collisional associations have been studied and shown to generate the protonated vinyl alcohol ion $H_2C{=}CHOH_2^+$, and possibly the protonated acetaldehyde ion, CH_3CHOH^+.[17] Neutral acetylene−water interactions including those in acetylene−water clusters have been the subject of both theoretical[18–22] and experimental studies.[23–26] Although in the neutral system acetylene can interact with water as a proton donor or proton acceptor, both experimental and theoretical studies show that the structure in which acetylene bonds as a proton donor is more stable energetically.[23] Similar results have been found in the interaction of acetylene with ice surfaces.[25]

The ionic reactions of acetylene and water, ($C_2H_2^{+\bullet}$/H_2O) can generate the association product $C_2H_4O^{+\bullet}$, which posseses several isomeric forms including covalent structures and simple ion−molecule electrostatic complexes such as $C_2H_2^{+\bullet}(H_2O)$. In the present work, mass-selected drift tube experiments coupled with ab initio calculations are used to examine the energies, structures and formation mechanisms of the product ions resulting from the reactions of the acetylene radical cation with water. We also investigate the energetics and structures of the hydrated product ions. This work initiates the first experimental investigation in this system and provides a comprehensive theoretical study of the energetics and structures of the relevant ions.

II. Experimental and Computational Methods

The experiments were carried out using the VCU mass-selected ion-mobility system. The details of the instrument have been published elsewhere,[27,28] and only a brief description is given here. Acetylene radical ions ($C_2H_2^{+\bullet}$) were generated by electron impact ionization (EI) of the clusters formed by supersonic beam expansions of 1–2% acetylene in helium mixtures. The ions were mass selected by a quadrupole mass filter and transported by a series of lenses into the ion mobility

* Corresponding author. E-mail: mselshal@vcu.edu.
† Permanent address: Department of Chemistry, University of Richmond, Richmond, VA 23173.

10.1021/jp802086z CCC: $40.75
Published on Web 06/18/2008

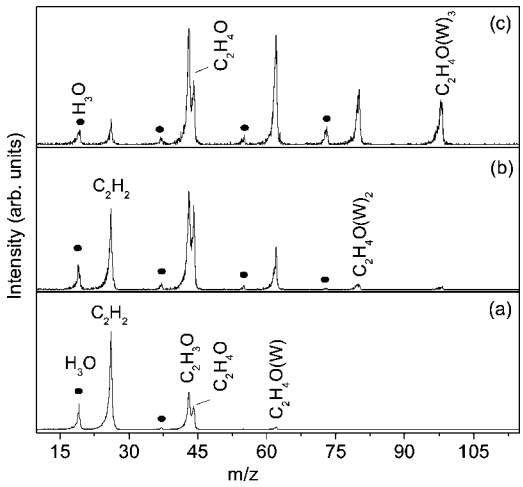

Figure 1. Mass spectra obtained following the injection of the $C_2H_2^{+\bullet}$ ions into the drift cell containing H_2O/He at 303 K, cell field 2.81 V/cm, $P(H_2O)$ = 20 mTorr, P(He) = (a) 358 mTorr, (b) 712 mTorr, and (c) 1441 mTorr. (•) denotes protonated water clusters $H_3O^+(H_2O)_n$.

cell, which was filled with pure H_2O vapor or mixtures of H_2O vapor and helium. Arrival time distributions (ATDs) or residence time of the various ions were measured by monitoring the signals corresponding to each ion as a function of time after injection into the cell. Residence time was varied between 200 and 1000 μs by changing the voltage gradient in the cell. Time-resolved studies allow the identification of primary and secondary reaction products and the measurement of rate coefficients. Pseudo-first-order rate constant (k_1) for the decay of the $C_2H_2^{+\bullet}$ reactant ions were obtained using the relation $\ln I/\Sigma I = -k_1 t$, where I is the integrated intensity of the reactant or product ion peak, ΣI is the sum of intensities of the reactant and all product ion peaks including secondary products, and t is the mean drift time of the reactant ion. The second-order rate coefficient, k_2, was obtained from relation, $k_2 = k_1/[N]$, where N is the number density of the reactant H_2O molecules in the cell.

Geometries and relative energies were calculated using the G3(MP2) method.[29] G3(MP2) is a composite method for accurate energy predictions; it follows HF and MP2 geometry optimizations with a sequence of high level single point energy calculations to improve the total energies.[29,30] The average absolute deviation of the G3(MP2)-predicted enthalpies from experimental values is 0.45 kcal/mol for molecules consisting of only C, H, and O atoms.[30] We also calculated the geometry and energy of the non-covalent $C_2H_2^{+\bullet}\cdot H_2O$ adduct. Finally, to gain further understanding of the experimental results, geometries and binding energies (BE) were calculated for selected $C_2H_4O^{+\bullet}\cdot H_2O$ and $C_2H_3O^+\cdot H_2O$ isomers. All calculations were performed using the Gaussian 03 suite of programs.[31]

III. Results and Discussion

1. Reaction Kinetics, Pressure and Temperature Effects. Figure 1 displays the mass spectra obtained following the injection of $C_2H_2^{+\bullet}$ into the drift cell containing mixtures of H_2O vapor and He at different pressures. The main ions are the remaining unreacted $C_2H_2^{+\bullet}$ (m/z = 26); the $C_2H_3O^+$ (m/z = 43); the $C_2H_4O^{+\bullet}$ (m/z = 44) and its hydrated adducts $C_2H_4O^{+\bullet}(H_2O)_n$ with n = 1−3 (m/z = 62, 80 and 98, respectively). In addition, a minor weak series of protonated water clusters $H^+(H_2O)_n$, HW_n, are also observed, apparently formed by high-energy collisions upon injection of the $C_2H_2^{+\bullet}$ ion.

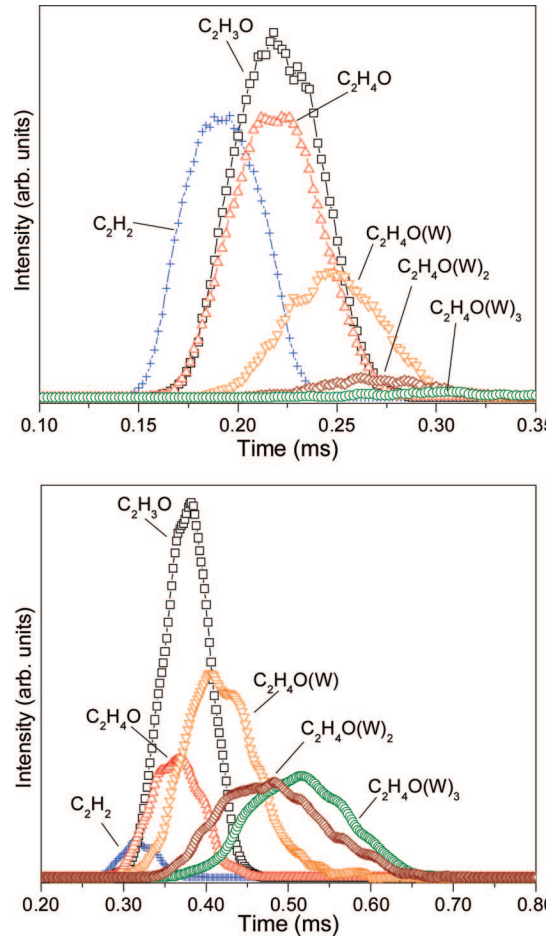

Figure 2. (Top) Arrival time distributions (ATDs) of the ions observed following the injection of the $C_2H_2^{+\bullet}$ ions into H_2O/He at 303 K, $P(H_2O)$ = 20 mTorr, P(He) = 712 mTorr. (Bottom) Arrival time distributions (ATDs) of the ions observed following the injection of the $C_2H_2^{+\bullet}$ ions into H_2O/He at 303 K, $P(H_2O)$ = 20 mTorr, P(He) = 1441 mTorr. In both figures, W denotes H_2O.

The primary products correspond to reactions 1 and 2, and the secondary products correspond to further reactions of the $C_2H_3O^+$ and $C_2H_4O^{+\bullet}$ ions with H_2O molecules. As shown in Figure 1, the ion intensity of the secondary hydrated products increases with increasing the He pressure in the drift cell.

$$C_2H_2^{+\bullet} + H_2O \rightarrow C_2H_4O^{+\bullet} \quad (1)$$

$$C_2H_2^{+\bullet} + H_2O \rightarrow C_2H_3O^+ + H \quad (2)$$

Examples of the the ATDs of the $C_2H_2^{+\bullet}$ and the product ions obtained at different He pressures are displayed in Figure 2. The ATDs show no overlap among the observed ions thus suggesting that the reactant and product ions are not in equilibrium. Equilibrium populations result in interchange among the coupled ions as they drift through the cell. The lack of equilibrium suggests that at least the first H_2O molecule adds irreversibly to $C_2H_2^{+\bullet}$ under our experimental conditions.

To test if the H atom loss (reaction 2) occurs from the H_2O moiety, we performed an isotope labeling experiment by injecting $C_2D_2^{+\bullet}$ (m/z 28) into the drift cell containing H_2O/He mixture. The resulting mass spectrum, shown in Figure 3, indicates the formation of a $C_2D_2HO^+$ ion (m/z 45) where the hydrogen loss occurred exclusively from the H_2O moiety. This suggests that at least the initial product of reaction 2 is an $HCCHOH^+$ ion formed by the addition of H_2O and the exclusive

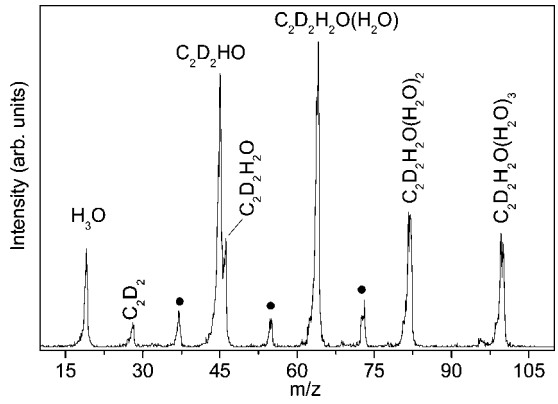

Figure 3. Mass spectrum obtained following the injection of the $C_2D_2^{+\bullet}$ ions into drift cell containing H_2O/He at 304 K, cell field 4.00 V/cm, $P(H_2O) = 20$ mTorr, $P(He) = 999$ mTorr. (•) denotes protonated water clusters $H_3O^+(H_2O)_n$.

H loss from the H_2O moiety without H/D scrambling in the intermediate complex.

The upper-left and upper-right sections of Figure 4 display examples of the time profiles of the reactant and product ions obtained at different He pressures and temperatures, respectively. The decay of the ion intensity of the reactant ions $C_2H_2^{+\bullet}$ and and the parallel formation of the $C_2H_3O^+$ and $C_2H_4O^+$ ions along with the hydrated products are clearly shown in Figure 4. The data clearly show that the product ratio $[C_2H_4O^+]/[C_2H_3O^+]$ increases with He pressure, and that the reaction efficiency increases with decreasing temperature.

We also observe $H^+(H_2O)$ clusters whose time profile can be decomposed into a time-independent component, apparently formed by high-energy collisions upon injection of the $C_2H_2^{+\bullet}$ ion, and a time-dependent component that increases at longer reaction times as shown in the bottom section of Figure 4. This increase occurs along with a compensating decrease in the $C_2H_3O^+$ ion, suggesting slow deprotonation of this ion by water to form the $H^+(H_2O)_n$ clusters.

To obtain structural information on the $C_2H_4O^{+\bullet}$ ion, we measured the reduced mobility of the mass-selected $C_2H_2D_2O^{+\bullet}$ ion generated by the EI ionization of binary $(C_2H_2)_n(H_2O)_m$ clusters formed by supersonic beam expansion of a C_2H_2/D_2O vapor mixture in He. The ATDs of the $C_2H_2D_2O^{+\bullet}$ ion using a helium buffer gas at a pressure (P) of 3.8 Torr (299 K) at different cell voltages are shown in Figure 5. The excellent linear plot of the mean arrival time vs. P/V (Torr V^{-1}) yields a reduced mobility (K_0) of 16.24 ± 0.5 $cm^2\ V^{-1}\ s^{-1}$ for the $C_2H_2D_2O^{+\bullet}$ ion. The reduced mobility is related to the average collision cross section (Ω) of the ion in the buffer gas through the kinetic theory.[27,28,32,33] The measured reduced mobility of the $C_2H_2D_2O^{+\bullet}$ ion corresponds to Ω of 34.5 ± 1.0 $Å^2$, which will be compared to calculated cross sections of other $C_2H_4O^{+\bullet}$ isomers obtained from the theoretical calculations presented in section 3. The calculated Ω of the $C_2H_4O^{+\bullet}$ isomers were obtained using the trajectory calculations which employ a potential consisting of LJ and ion-induced dipole interactions.[33]

The time resolved study shown in Figure 4 suggests a reaction mechanism summarized in Scheme 1, and is further supported by the data shown in Table 1, which summarizes the results obtained from the kinetic measurements.

From the analysis of the data shown in Table 1, the following features can be identified:

1. The second-order rate coefficient for the overall reaction is independent of water concentration within the experimental uncertainty (±30 %). In other words, the reaction is first order with respect to H_2O as indicated in Scheme 1.

2. The rate coefficient for the overall reaction to form products is on the order of 2.0(±0.6) × 10^{-11} $cm^3\ s^{-1}$ at 300 K, which

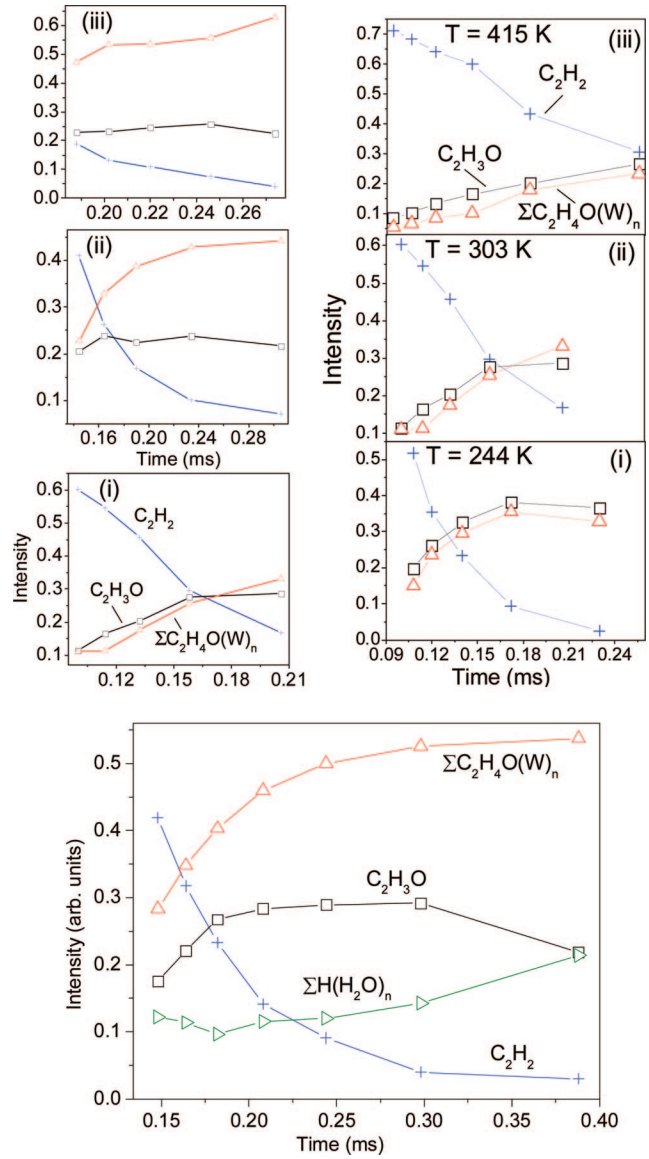

Figure 4. (Upper left) Normalized intensities of ion signals (integrated ATD peaks) as a function of reaction time following the injection of the $C_2H_2^{+\bullet}$ ions into the drift cell with $P(H_2O) = 20.0$ mTorr (or $N[H_2O] = 6.6 \times 10^{14}$ molecules/cm^3), $T = 303.3$ K. The helium partial pressure was (i) 358.0 mTorr ($N[He] = 1.18 \times 10^{16}$ molecules/cm^3), (ii) 712.0 mTorr ($N[He] = 2.34 \times 10^{16}$ molecules/cm^3) and (iii) 1439.0 mTorr ($N[He] = 4.73 \times 10^{16}$ molecules/cm^3). W_n denotes H_2O and $C_2H_4O^{+\cdot}$ $(W)_n$ denotes the combined intensities of the $n = 0-4$ ions. The intensities are normalized to the sum of the reactant and all product ions. (Upper right) Normalized intensities of ion signals (integrated ATD peaks) as a function of reaction time following the injection of the $C_2H_2^{+\bullet}$ ions into the drift cell with $P(H_2O) = 20$ mTorr (or $N[H_2O] = 6.6 \times 10^{14}$ molecules/cm^3). The temperature and helium partial pressure were (i) 244.1 K and 311.0 mTorr ($N[He] = 1.27 \times 10^{16}$ molecules/cm^3), (ii) 303.3 K and 358.0 mTorr ($N[He] = 1.18 \times 10^{16}$ molecules/cm^3) and (iii) 414.9 K and 371.0 mTorr ($N[He] = 8.92 \times 10^{15}$ molecules/cm^3). (Bottom) Normalized intensities of ion signals (integrated ATD peaks) as a function of reaction time following the injection of the $C_2H_2^{+\bullet}$ ions into the mobility cell with $P(H_2O) = 20$ mTorr (or $N[H_2O] = 7.19 \times 10^{14}$ molecules/cm^3), $T = 272$ K. The helium partial pressure was 1002.0 mTorr ($N[He] = 3.68 \times 10^{16}$ molecules/cm^3). W denotes H_2O and $C_2H_4O^{+\cdot}$ $(W)_n$ denotes the combined intensities of the $n = 0$–4 ions.

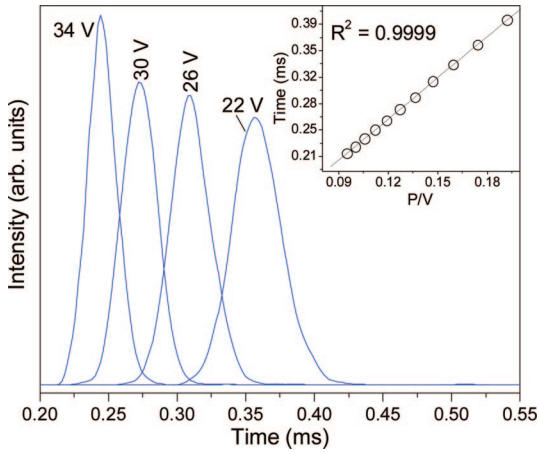

Figure 5. Arrival time distributions (ATDs) of the $C_2H_2D_2O^{+\bullet}$ ion at different drift voltages. The temperature of the drift cell was 299 K and the pressure of the helium buffer gas (P) was 3.8 Torr. The inset shows a plot of the mean arrival time of $C_2H_2D_2O^{+\bullet}$ as a function of P/V (Torr V^{-1}).

SCHEME 1

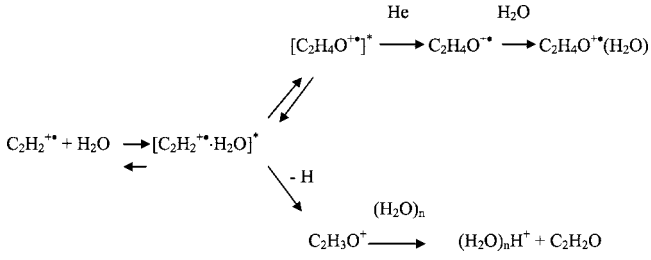

is about 2 orders of magnitude smaller than the collision rate (10^{-9} cm^3 s^{-1}). This suggests that back-dissociation of the excited complex $[C_2H_2^{+\bullet}\cdot H_2O]^*$ occurs at a rate faster by about a factor of 100 than the forward reaction to products.

3. The reaction efficiency decreases with increasing temperature. The temperature dependence of the rate coefficient is well fit by a power law with $T^{-2.4}$ dependence which is the normal range for such reactions.[34] The negative temperature dependence is a result of the back-dissociation of the excited complex, $[C_2H_2^{+\bullet}\cdot H_2O]^*$, which becomes faster and competes more efficiently with the forward reaction at higher temperatures.

4. The product ratio $[C_2H_4O^{+\bullet}]/[C_2H_3O^+]$, adduct formation vs H atom loss, increases with third-body pressure, P(He) (see Figure 4, upper left), and with decreasing temperature (Table 1 and Figure 4, upper right). These trends are consistent with reaction through an excited complex that is stabilized collisionally to form an adduct, and whose rate of dissociation increases with increasing temperature. However, the rate coefficient for the H atom loss channel, $k(C_2H_3O^+)$, appears to decrease at higher third-body pressure. Because the overall rate coefficient k_f appears to be not affected by P(He), this implies that the association channel, $k(C_2H_4O^+)$, competes for reactivity with the H-loss channel (two-body). This is unusual because rates of reactions for which $k_f \ll k_{collision}$ usually increase with third-body pressure.[34] It also appears that the pressure dependences for the reaction channels do not extrapolate to zero at zero pressure. This implies that the association channel, $k(C_2H_4O^+)$, may have both radiative and third-body stabilizations. These observations suggest that the mechanism for Scheme 1 requires further analysis.

5. The $C_2H_3O^+$ product is deprotonated by water to form $(H_2O)_nH^+$ cluster ions (Figure 4, bottom). This reaction becomes more pronounced with increasing $P(H_2O)$. In fact, when $C_2H_2^{+\bullet}$ was injected into neat H_2O vapor at > 100 mTorr, we did not observe the $C_2H_3O^+$ ion but only $(H_2O)_nH^+$ cluster ions.

2. Thermochemical Estimates for the $C_2H_4O^{+\bullet}$ Adduct Ion. The association reaction $C_2H_2^{+\bullet} + H_2O \rightarrow C_2H_4O^{+\bullet}$ was irreversible under all of our experimental conditions reaching, for example, a product/reactant ion ratio $[C_2H_4O^{+\bullet}]/[C_2H_2^{+\bullet}]$ of 16.8 at the longest reaction time observed at 363 K. If the reaction proceeded further toward equilibrium, the product/reactant ion ratio should increase further. In other words, the observed ratio is the lower limit of the equilibrium product/reactant ion ratio. From this we can calculate a limit of $\Delta G°_{(363K)}(\text{association}) = -RT \ln K_{(363)} < [C_2H_4O^{+\bullet}]/([C_2H_2^{+\bullet}]P(H_2O)) = -RT \ln(16.8/2.8 \times 10^{-5}\ (\text{atm})) = -9.6$ kcal/mol. If the adduct was a hydrogen-bonded cluster, we could assume $\Delta S°(\text{association}) \sim -20$ cal/(mol K) giving at 363 K the value of $\Delta H°(\text{association}) = \Delta G°(\text{association}) + T\Delta S°(\text{association}) < -16.9$ kcal/mol as the lower limit of the binding energy. This is somewhat larger than the binding energies for cluster ions of the type $CH^{\delta+}\cdots OH_2$ where binding energies are usually 10−14 kcal/mol.[35]

If the adduct is covalently bonded, we may assume $\Delta S° \sim -40$ cal/mol K, and using the same limiting $\Delta G°_{(363)}(\text{association}) < -9.6$ kcal/mol above would yield $\Delta H°(\text{association}) < -24.1$ kcal/mol. This is consistent with forming covalent $C_2H_4O^{+\bullet}$ isomers such as c-$(CH_2{=}CH_2{-}O)^{+\bullet}$, $CH_3CHO^{+\bullet}$ or $H_2C{=}CH{-}OH^{+\bullet}$ with exothermicities of 28.3, 64.2, or 74.7 kcal/mol, respectively.[36] Note, however, that the products may not be the most stable isomers if their formation involves significant energy barriers.

3. Theoretical Calculations of the $C_2H_4O^{+\bullet}$ and $C_2H_3O^+$ Isomers. These calculations are concerned with the energies and geometries of isomers of the $C_2H_4O^{+\bullet}$ and $C_2H_3O^+$ ions and their complexes with H_2O. The calculations identify low energy isomers that may be the observed species and rule out some alternative structures. Energies and structures of the $C_2H_5O^+$ ion that also form in acetylene/water reactions (not observed under our conditions) have been studied previously.[17]

$C_2H_4O^{+\bullet}$. The G3 (MP2) results on the $C_2H_4O^{+\bullet}$ hypersurface are summarized in Table 2. Experiment-based values, when available, are shown in brackets. As shown in Table 2, the calculated energies of reaction 1, ΔE_r, are in excellent agreement with the experimental values for most of the $C_2H_4O^{+\bullet}$ isomers thus confirming that the G3(MP2) method is satisfactory for this system.

The lowest energy structure of the $C_2H_4O^{+\bullet}$ ion is the ethenolium cation $H_2C{=}CHOH^{+\bullet}$ (**2a**; absolute G3(MP2) energy = −153.239 au), followed by the acetaldehyde cation $CH_3CHO^{+\bullet}$ (**2b**), which is 13.3 kcal/mol less stable than **2a**. The cyclic ethylene oxide cation (**2h**) is predicted to be much higher in energy than **2a** (48.7 kcal/mol). The (methyliumoxy)methyl ion $H_2COCH_2^{+\bullet}$ (**2d**) with a relative energy of 26.0 kcal/mol is predicted to be 22.7 kcal/mol more stable than its potential cyclic precursor ion (**2h**).[37] Several other species, including 1-hydroxy-1-ethylium-1-yl (**2c**), 16.4 kcal/mol; methyloxoniumylidenylmethyl (**2e**), 35.4 kcal/mol; *cis*-HC-$CHOH_2^{+\bullet}$ cation (**2f**), 44.4 kcal/mol, and *trans*-$HCCHOH_2$ cation (**2g**), 44.5 kcal/mol are predicted at the G3(MP2) level to be more stable than **2h**. The unstable $CH_2CH_2O^{+\bullet}$ ion converged to **2h** upon optimization. This is in agreement with previous suggestion that the $CH_2CH_2O^{+\bullet}$ species, if formed, isomerizes to **2d** via **2h**.[37]

The $C_2H_2^{+\bullet}\cdot H_2O$ complex **2k** was the highest energy species we investigated on the hypersurface, with a relative energy of

TABLE 1: Pressure and Temperature Effects on the Rate Coefficients and Product Ratios in the $C_2H_2^{+\bullet}$ + H_2O Reaction System

T (K)	$P(H_2O)$ [a]	P(He) [a]	k_f [b]	product ratio $r = [C_2H_4O^{+\bullet}]/[C_2H_3O^+]$ [c]	k [d] ($C_2H_3O^+$)	k [d] ($C_2H_4O^{+\bullet}$)
			Water Pressure Study			
303	10.0	370	24	0.8	13.2	10.4
303	15.5	362	21	1.0	10.6	10.2
303	21.5	370	20	0.9	10.4	9.6
304	20.6	357	21	0.9	10.9	10.0
303	26.0	349	20	1.0	10.2	9.8
303	35.0	331	19	0.9	10.1	9.1
			Helium Pressure Study			
303	21.5	370	20	0.9	10.4	9.6
303	20.0	712	23	1.4	9.6	13.6
304	20.6	999	22	1.4	9.1	12.4
303	20.0	1002	24	1.6	9.3	14.4
303	20.0	1441	26	2.2	8.0	17.5
			Temperature Study[e]			
244	18.6	293	32.4	0.9	17.3	15.1
272	19.6	332	26.2	0.8	14.9	11.3
303	21.5	370	20	0.9	10.4	9.6
331	21.9	366	16.0	0.6	10.2	5.8
359	22.9	362	12.8	0.5	8.4	4.4
415	24.5	372	9.2	0.6	5.6	3.6

[a] Units in mTorr. [b] Rate coefficients for the overall forward reaction $C_2H_2^{+\bullet}$ + H_2O → products in units of 10^{-12} cm^3 s^{-1}. Estimated uncertainty in rate coefficient measurements is usually ±30 %. [c] Product ion ratio. The hydrated products $C_2H_4O^{+\bullet}(H_2O)_n$ are considered secondary products of the primary adduct channels and their intensities are included in the $C_2H_4O^{+\bullet}$ adduct ion intensities. [d] Rate coefficients based on product channel ratios. Calculated from the rate coefficients in column 4 and product ion ratios r in column 5 according to $k(C_2H_3O^+) = k_f(1/(1 + r))$ and $k(C_2H_4O^{+\bullet}) = k_f(r/(1 + r))$. In units of 10^{-12} cm^3 s^{-1} [e] Experiments using $C_2D_2^{+\bullet}$ ions. The temperature study was conducted at constant number densities of $N[H_2O] = 6.76(\pm0.6) \times 10^{14}$ molecules/cm^3 and N[He] = $1.12(\pm0.1) \times 10^{16}$ molecules/cm^3.

58.1 kcal/mol. The corresponding $HCCH^{+\bullet}\cdots OH_2$ binding energy is predicted to be 17.6 kcal/mol, which is reasonable for a $CH^{\delta+}\cdots O$ type hydrogen bond although it represents the highest range for such bonds. However, this complex is predicted as stable only when constrained to C_{2v} symmetry. Any deviation from the C_{2v} symmetry results in a covalent addition of water to the acetylene cation, thus forming the *trans*-$HCCHOH_2^{+\bullet}$ cation (**2g**). The hydrogen-bonded complex, **2k**, may be an intermediate in the covalent association reaction, proceeding to an excited **2g** ion with an internal energy of ΔE_r = 13.6 kcal/mol, which then allows it to overcome energy barriers and to rearrange to a more stable isomer.

It should be noted that the calculated collision cross-section (Ω) of the $C_2H_2^{+\bullet}\cdot H_2O$ complex (isomer **2k**) in He (39.9 Å^2) is sufficiently different from the value measured for the $C_2H_4O^{+\bullet}$ ion (34.5 Å^2, Figure 5). This allows us to exclude isomer **2k** and to conclude that the observed $C_2H_4O^{+\bullet}$ ion has a covalent structure. The calculated Ω values of all the covalent structures (isomers **2a** to **2j** in Table 2) range from 33 to 36 Å^2, which are similar to the measured Ω of the $C_2H_4O^{+\bullet}$ ion (within the experimental error) but different from Ω of the $C_2H_2^{+\bullet}\cdot H_2O$ ion−molecule complex. As will be discussed later in this text, experimental and theoretical considerations point to **2a** as the most likely $C_2H_4O^+$ ion.

$C_2H_3O^+$. Table 3 summarizes the predicted $C_2H_3O^+$ geometries and thermochemistry. In all, seven stable species were found on the potential hypersurface. The most stable species, is, as expected, 1-oxo-ethylium (acetyl, (**3a**) CH_3CO^+) followed by 1-hydroxyethenylium (protonated ketene, **3b**; CH_2COH^+), 41.6 kcal/mol higher in energy. Two stable structures with COC heavy atom skeletons were also found. They are methyloxoniumylidenemethylene (**3c**) and methyleneoxoniomethylene (**3g**) with relative energies of 54.5 and 106.5 kcal/mol, respectively. The fourth most stable $C_2H_3O^+$ isomer is 2*H*-oxirenylium (**3d**; *c*-$CHCH_2O^+$), with a relative energy of 55.9 kcal/mol. The relative stability of **3a**, **3b**, and **3d** is predominantly governed by the site of protonation if one considers the neutral ketene ($H_2C_\beta{=}C_\alpha{=}O$) as a precursor. Structural details of the $H_2C{=}C{=}O$ ion have been discussed by Ma and Wong.[38] The electrostatic attraction between the $C_\beta^{\delta-}$ and $O^{\delta+}$ atoms as a result of the resonance, $H_2C_\beta{=}C_\alpha{=}O \leftrightarrow H_2C_\beta^{\delta-}{-}C_\alpha'O^{\delta+}$ helps to stabilize **3d** by formation of a C−O bridge.

A cyclic $CHCHOH^+$ ion (**3e**) and ethynyloxonium ion (**3f**) are also found to be stable with relative energies 82.4 and 82.6 kcal/mol, respectively. Previous work at the MP2/6-31G** level also predicted **3e** and **3f** as stable structures with relative energies of 83.7 and 85.3 kcal/mol, respectively, in good agreement with our results.[39] Calculated ΔE_r for the reaction show the formation of isomers **3c** to **3g** to be endothermic, leaving **3a** and **3b** as the most probable isomers. However, thermochemical data from the NIST database[36] shows the formation of **3d** to be moderately exothermic (−6.2 kcal/mol). Also, previous experiments have suggested that **3d** may be a stable/observable $C_2H_3O^+$ isomer.[40]

Optimization of the acyclic CH_2CHO^+ (formylmethyl cation) species converged to **3d** at the G3(MP2) level of theory. Previous calculations at the MP3/6-31G(d,p) level of theory predicted the formylmethyl cation to be stable though 20.6 kcal/mol less stable than **3d**.[39] This suggests that the formylmethyl cation is not the experimentally observed $C_2H_3O^+$ isomer. Although we tried a substantial number of starting geometries, including all known neutral isomers of C_2H_3O, at the G3(MP2) level of theory, they all relaxed to one of the seven isomers reported in Table 3.

4. Formation and Deprotonation of the $C_2H_3O^+$ Product Ion. The $C_2H_3O^+$ product ion is formed through hydrogen atom loss from the reactants ($C_2H_2^{+\bullet}$ + H_2O). The stable isomers are CH_3CO^+ (1-oxo-ethylium/acylium), $H_2C{=}C{=}OH^+$ (1-hydroxy-ethenylium or O-protonated ketene), a linear or cyclic CH_2CHO^+ (C_α-protonated ketene) and a linear or cyclic $HCCHOH^+$ ion. As for the thermochemistry of reaction , experimental reaction enthalpies ($\Delta H_r°$)[36] show the formation of the acylium (Table 3a) isomer to be exothermic by 49.2 kcal/

TABLE 2: G3(MP2) Calculated Structures and Energies of $C_2H_4O^{+\bullet}$ Isomers[a]

	Isomer Cation	Structure	Bond Lengths (Å) and Angles (°)[b]	Relative Energy[c]	ΔE_r(298K)[c,d,e]
a	Ethenolium (Vinyl Alcohol)	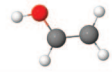	rC-C = 1.41 rC-O = 1.29 CCO = 117.4	0.0[i]	-75.7 [-75.4]
b	Acetaldehyde cation		rC-C = 1.49 rC-O = 1.22 CCO = 123.0	13.3 [13][g,h]	-62.4 [-62.6]
c	1-hydroxy-1-ethylium-1-yl		rC-C = 1.45 rC-O = 1.25 CCO = 128.5	16.4	-59.4
d	(Methyliumoxy)-methyl		rC_1-O = 1.27 rC_2-O = 1.36 COC = 124.5	26.0 [22][g,h]	-49.7 [-57.3]
e	Methyloxononiumylidene-methyl		rC_1-C = 1.54[f] rC_2-O = 1.22 COC = 124.5	35.4 [40][g,h]	-40.3 [-35.3]
f	Cis-$HCCHOH_2$	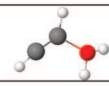	rC-C = 1.26 rC-O = 1.57 CCO = 120.2	44.4	-31.4
g	Trans-$HCCHOH_2$		rC-C = 1.27 rC-O = 1.55 CCO = 116.1	44.5	-31.3
h	Ethylene oxide	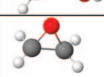	rC-C = 1.46 rC-O = 1.49 CCO = 60.7	48.7 [47][g,h]	-27.1 [-28.3]
i	H_2CCOH_2	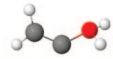	rC-C = 1.28 rC-O = 1.46 CCO = 123.9	49.6	-26.1
j	Cyclic CH_2CHOH		rC-C = 1.44 rC-O = 1.56 CCO = 59.1	50.8	-25.0
k	$C_2H_2^+ \cdot H_2O$		rC-C = 1.26 $rC\text{-}OH_2$ = 2.8	58.1	-17.2

[a] The G3(MP2) method was utilized. Experimental numbers are shown in brackets. [b] Bond lengths and angles for select bonds. [c] kcal/mol. [d] Energy of reaction 1 at 298 K. [e] Using $\Delta H°_f(C_2H_2^{+\bullet}) = \Delta H°_f(C_2H_2) + IE(C_2H_2) = 54.19 + 262.88 = 317.1$ kcal/mol and $\Delta H°_f(H_2O) = -57.80$ kcal/mol from NIST Database.[36] [f] C_1 is the methyl carbon. [g] Experimental heat of formation for **2a** is 184 kcal/mol.[36] Other numbers shown are relative to this value. $\Delta H_f°$ for **2a**, **2b**, and **2h** were obtained from NIST Database[35] and $\Delta H_f°$ for **2d** and **2e** were obtained from work of Terlouw et al.[40] [h] Relative energies obtained by the difference in experimental $\Delta H_f°$. [i] Calculated G3(MP2) absolute energy of **2a** is −153.239 au.

mol and theoretical reaction energies (ΔE_r) show the formation of both the acylium and 1-hydroxyethenylium (**3b**) isomers to be exothermic by 50.2 and 8.6 kcal/mol, respectively. The formation of **3d** is endothermic according to the G3(MP2) calculations and is slightly exothermic (6.2 kcal/mol) according to the thermochemical data from the NIST database.[36]

If the most stable $C_2H_3O^+$ isomer (CH_3CO^+) is formed in our experiments, it would react with water to give $CH_3COOH_2^+$, i.e., protonated acetic acid,[41] which then forms hydrated $CH_3COOH_2^+(H_2O)_n$ clusters with further H_2O molecules, which were not observed in our experiments. This indicates that the experimentally observed $C_2H_3O^+$ isomer in our experiments is not the CH_3CO^+ ion. This leaves isomer **3b** as the most likely structure of the $C_2H_3O^+$ ion formed by an exothermic reaction (reaction 2). It should be noted, however, that the formation of either isomer **3b** or **3d**, unlike the formation of isomer **3c**, does not require breaking the acetylene CC bond.

The observed reactivity provides further information on the structure of the $C_2H_3O^+$ ion. This ion seems to be deprotonated slowly by water to form $H^+(H_2O)_n$ clusters. This is shown in Figure 4 (bottom) where the decrease in the $C_2H_3O^+$ ion population is compensated for by a simultaneous increase of the intensity of the $H^+(H_2O)_n$ clusters, but only at long reaction times, suggesting slow deprotonation. We observed similar reactions in the deprotonation of the hydrocarbon ions $C_6H_6^{+\bullet}$ (benzene cation) and c-$C_3H_3^+$ that were deprotonated by several H_2O molecules to form $(H_2O)_nH^+$ cluster ions.[35,42] The driving force for this reaction is the replacement of the weak $CH^{\delta+}\cdots OH_2$ hydrogen bonds between the ions and H_2O by a network of stronger $OH^+\cdots OH_2$ ionic hydrogen bonds in the $H^+(H_2O)_n$ clusters. Both isomers **3b** and **3d** can form H-bonding with water molecules that could lead to dissociative proton transfer to form $H^+(H_2O)_n$ clusters. However, the deprotonation of isomer **3b** is expected to be fast because the proton affinity of H_2O (165 kcal/mol) is higher than the calculated proton affinity at the O site of the neutral ketene (153.7 kcal/mol) corresponding to the deprotonated structure of isomer **3b**. On the other hand, the deprotonation of isomer **3d** is expected to be slow because it involves breaking of a C−H bond following the H-bonding with several water molecules. Because the formation of $H^+(H_2O)_n$ clusters in our experiments occurs only at long reaction times (Figure 4, bottom), this may suggest that the observed $C_2H_3O^+$ ion population may contain a contribution from the c-$[CH_2CHO]^+$ structure (isomer **3d**).

5. Calculated Energies and Geometries of $C_2H_4O^+ \cdot H_2O$ and $C_2H_3O^+ \cdot H_2O$ Complexes. To gain more insight into the solvation and reactions of the $C_2H_4O^{+\bullet}$ and $C_2H_3O^+$ ions, we calculated the geometries and binding energies (BE) for selected $C_2H_4O^{+\bullet} \cdot H_2O$ and $C_2H_3O^+ \cdot H_2O$ complexes. The stable geometries for the selected complexes are shown in Figure 6. Two

TABLE 3: G3(MP2) Results on Isomers of $C_2H_3O^+$[ah]

	Isomer	Structure	Bond Lengths (Å) and Angles (°)	Relative Energy[b,e]	ΔE_r(298K)[b,c,d]
a	1-oxo-ethylium/Acylium (Acetyl cation)		rC-C = 1.42 rC-O = 1.13 CCO = 180.0	0.0[f]	-50.2 [-49.2,[g] -50.2[h]]
b	1-hydroxy-ethenylium (1-hydroxyvinyl cation)		rC-C = 1.28 rC-O = 1.23 CCO = 174.5	41.6	-8.6
c	Methyloxoniumylidene-methylene		rC_1-O = 1.57[k] rC_2-O = 1.17 COC = 180.0	54.5	4.4
d	2H-oxirenium (Oxiranyl cation)		rC-C = 1.44 rC_β-O = 1.64[i] $CC_\beta O$ = 47.4	55.9 [43]	5.7 [-6.2][j]
e	Cyclic CHCHOH/Protonated Oxirene		rC-C = 1.27 rC-O = 1.56 COC = 48.3	82.4	32.2
f	Ethynyloxonium		rC-C = 1.21 rC-O = 1.38 CCO = 177.4	82.6	32.4
g	Methyleneoxonio-methylene		rC_1-O = 1.29[l] rC_2-O = 1.25 COC = 166.6	106.5	56.3

[a] The G3(MP2) method was utilized. Experimental numbers are shown in brackets. [b] In kcal/mol. [c] Energy of reaction 2 at 298 K. [d] Using $\Delta H_f°$ for $C_2H_2^{+\bullet}$ = 317.1 kcal/mol; for $H^\bullet$ = 52.1 kcal/mol; and for H_2O = −57.8 kcal/mol. [e] Using $\Delta H_f°$(**3a**) = 158.5 kcal/mol and $\Delta H_f°$(**3d**) = 201 kcal/mol based on NIST values. Other numbers shown are relative to **3a**. [f] Calculated G3(MP2) absolute energy of **3a** is −152.698 au. [g] Obtained using $\Delta H_f°(CH_3CO^\bullet)$ = −2.9±0.7 kcal/mol and IE ($CH_3CO^\bullet$) = 161.4 kcal/mol. [h] Obtained using $\Delta H_f°(H_2CCO)$ = −11.4 kcal/mol and PA(H_2CCO) = 197.3 kcal/mol for deprotonation on C. [i] C_β is the $-CH_2$ carbon. [j] Obtained using $\Delta H_f°$(*c*-H_2CCHO^+) = 201 kcal/mol. [k] C_1 is the methyl carbon. [l] C_1 is the $-CH_2$ carbon.

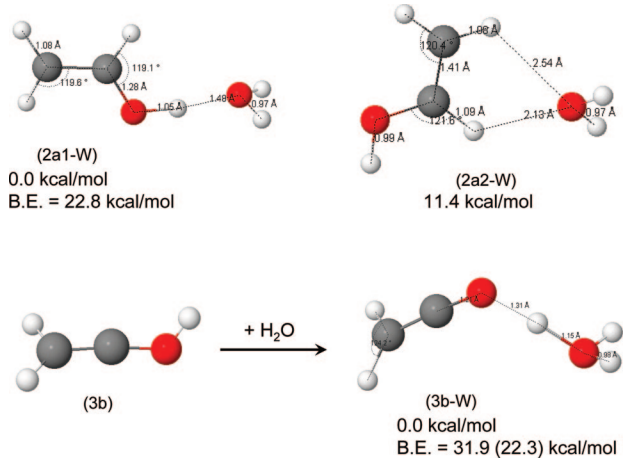

Figure 6. Structures, relative energies and binding energies (BE) of the $C_2H_4O^{+\bullet}(H_2O)$ (**2a1-W** and **2a2-W** isomers) and $C_2H_3O^+(H_2O)$ (**3b-W** isomer) complexes.

stable structures (**2a1-W** and **2a2-W**) are found for the hydrated ethenolium ion. Complex **2a1-W** consists of a water molecule hydrogen bonded (BE = 22.8 kcal/mol) to the OH group of **2a** with $r(OH\cdots OH_2)$ with a bond length of 1.48 Å. Complex **2a2-W**, 11.4 kcal/mol less stable than **2a1-W**, consists of the water molecule weakly bound (11.3 kcal/mol) to the C_α hydrogen with a longer $r(C_\alpha H\cdots OH_2)$ bond of 2.13 Å. This is consistent with the usual trend in ionic hydrogen bonds where the $OH^+\cdots OH_2$ bond such as in **2a1-W** is usually stronger than the $CH^{\delta+}\cdots OH_2$ bond such as in the **2a2-W** complex.[35,42,43] The large binding energy for **2a1-W** is in agreement with our experimental observation of $C_2H_4O^{+\bullet}\cdot(H_2O)_n$ even at high temperatures, whereas the more weakly bonded **2a2-W** should not have been observed at these temperatures. For example, using the calculated binding energy of 11.3 kcal/mol, typical association entropy of −20 cal/(mol K), temperature of 415 K (highest temperature used in experiment), and $P(H_2O)$ of 3.32×10^{-5} atm, an adduct/monomer ion ratio, $I(C_2H_4O^{+\bullet}\cdot H_2O)/I(C_2H_4O^{+\bullet})$, of 0.0013 is calculated. The experimental ratio at the same temperature and pressure was 0.5, approximately 385 times larger. Using the temperature, water pressure, and the $I(C_2H_4O^{+\bullet}\cdot H_2O)/I(C_2H_4O^{+\bullet})$ ratio above (0.5), the limit of $\Delta G°_{(415K)}$(association) = $-RT$ ln $K_{(415K)}$ = −9.1 kcal/mol. Then, the enthalpy of association should be $\Delta H°$(association) = $\Delta G°$(association) + $T\Delta S°$(association) < −17.4 kcal/mol. This lower limit for the binding energy is consistent with the 22.8 kcal/mol value calculated for **2a1-W**.

We can therefore draw conclusions about the structural identity of the $C_2H_4O^{+\bullet}$ ion calling on experimental and theoretical observations. The high binding energies for **2a1-W** is consistent with the estimated binding energy >17.4 kcal/mol (lower limit) for the observed $C_2H_4O^+\cdot H_2O$ complex. This result along with the calculated and experiment-based ΔE_r values (Table 2) suggest that isomer **2a** is the $C_2H_4O^+$ isomer observed in our experiments.

$C_2H_3O^+\cdot H_2O$. Because isomer **3a** is known to form protonated acetic acid and its hydrated clusters upon addition of water,[41,44] which we did not observe, we did not attempt any calculation for this species. The most interesting result was seen for the 1-hydroxyethenylium (**3b**)/water complex, CH_2-$COH^+\cdot H_2O$ (**3b-W**). As shown in Figure 6, the predicted geometry involves a complex in which the −OH hydrogen of **3b** migrates to the H_2O oxygen thus forming a neutral ketene molecule and a protonated water ion, ($CH_2CO\cdots H_3O^+$). The optimized $CH_2CO\cdots HOH_2^+$ bond length is 1.31 Å as compared to 1.0 Å for the unhydrated ion, **3b**. The OH bond lengths of H_3O^+ are 0.98, 0.98, and 1.15 Å (abstracted proton). Inspection of the atomic charge densities reveals a majority (92%) of total charge transfer to the H_3O^+ ion. The $CH_2CO\cdots H_3O^+$ binding energy (dissociation into CH_2CO + H_3O^+) for **3b-W** is calculated to be 22.3 kcal/mol. Although intracomplex proton

transfer does not necessary lead to intermolecular proton transfer, the latter process was experimentally observed as shown in Figure 4, bottom where, at long residence times, the $C_2H_3O^+$ ion intensity dropped with a corresponding increase in $(H_2O)_nH^+$ ion intensity. Comparison of the calculated proton affinities at the O site of neutral ketene, 153.7 kcal/mol with the proton affinities for n H_2O molecules (165, 197 and 217 kcal/mol for $n = 1$, 2, and 3, respectively)[36] indicates that proton abstraction reaction from **3b** to form protonated water clusters is thermochemically allowed. As noted above, calculated PAs for isomers **3b** and **3d** indicate both isomers can be deprotonated by water, consistent with the observed reactivity.

IV. Conclusions

The acetylene radical cation, $C_2H_2^{+\bullet}$, reacts with H_2O vapor by association to produce the $C_2H_4O^{+\bullet}$ adduct and $C_2H_3O^+$ by H atom loss. As often observed in ion-molecule reactions, the overall rate coefficient increases with decreasing temperature and the adduct/H loss product ratio increases with decreasing temperature and increasing third-body pressure.

The association reaction appears irreversible under our conditions and thermochemical estimates suggest that it produces a covalent $C_2H_4O^{+\bullet}$ ion which forms clusters with further H_2O molecules, $C_2H_4O^{+\bullet}(H_2O)_n$. Ab initio calculations show the lowest energy $C_2H_4O^{+\bullet}$ isomer to be the ethenolium (vinyl alcohol) ion, $H_2CCHOH^{+\bullet}$ which can form strong hydrogen bonds with water molecules, consistent with the observed results. Also, the formation of $H_2CCHOH^{+\bullet}$ from the $C_2H_2^{+\bullet}$ and H_2O reactants requires only a single H atom shift. These considerations suggest that the observed $C_2H_4O^{+\bullet}$ ion is the $CH_2{=}CHOH^{+\bullet}$ isomer.

The mechanism of formation of the $C_2H_3O^+$ product by H atom loss was confirmed by isotopic labeling as the H loss exclusively occurred from the H_2O reactant. The combination of energetics and reactivity indicates that the protonated ketene CH_2COH^+ is the most likely observed $C_2H_3O^+$ ion probably with some contribution from the cyclic c-CH_2CHO^+ ion. The hydration of the $C_2H_3O^+$ ion involves intracluster proton transfer followed by reactions with further H_2O molecules that lead to full deprotonation forming $H^+(H_2O)_n$ cluster ions and the neutral ketene CH_2CO.

The isomers identified by the theoretical calculations may form by ionic reactions in astrochemical environments or as intermediates and products in the dissociation of larger ions. Experiments and theoretical studies of these ions and their neutral counterparts are useful for modeling these environments.

Acknowledgment. This research was supported by grants from the National Science Foundation (CHE-0414613) and NASA (NNX07AU16G).

References and Notes

(1) Brooke, T. Y.; Tokunaga, A. T.; Weaver, H. A.; Crovisier, J.; Bockelee-Morvan, D.; Crisp, D. *Nature* **1996**, *383*, 606.

(2) Cernicharo, J.; Heras, M.; Tielens, A. G. G. M.; Pardo, J. R.; Herpin, F.; Guelin, M.; Waters, L. B. F. M. *Astrophys. J.* **2001**, *546*, L123.

(3) Scott, G. B. I.; Fairley, D. A.; Freeman, C. G.; McEwan, M. J.; Adams, N. G.; Babcock, L. M. *J. Phys. Chem. A* **1997**, *101*, 4973.

(4) Woods, P. M.; Millar, T. J.; Zulstra, A. A.; Herbst, E. *Astrophys. J.* **2002**, *574*, L167.

(5) Anicich, V.; McEwan, M. J. *Planet. Space Sci.* **1997**, *45*, 897.

(6) Woods, P. M.; Millar, T. J.; Herbst, E.; Zijlstra, A. A. *Astron. Astrophys.* **2003**, *402*, 189.

(7) Lewis, J. S.; Hutson, M. L. Chemistry of the Solar Nebula In *Chemistry in Space*; Greenberg, J. M., Pirronnello, V., Eds.; NATO ASI Series; Kluwer: Dordrecht, The Netherlands, 1989; p 321.

(8) Winnewisser, G.; Kramer, C. *Space Sci. Rev.* **1999**, *90*, 181.

(9) Ehrenfreund, P.; Irvine, W.; Becker, L.; Blank, J.; Brucato, J.; Colangeli, L.; Derenne, S.; Despois, D.; Dutrey, A.; Fraaije, H.; Lazcano, A.; Owen, T.; Robert, F. *ISSI-Team. Rep. Prog. Phys* **2002**, *65*, 1427.

(10) Williams, D. A.; Herbst, E. *Surf. Sci.* **2002**, *500*, 823.

(11) Fraser, H. J.; McCoustra, M. R. S.; Williams, D. A. *Astron. Geophys.* **2002**, *43*, 10.

(12) Somogyi, A.; Oh, C. H.; Smith, M. A.; Lunine, J. I. *J. Am. Soc. Mass Spectrom.* **2005**, *16*, 850.

(13) Turner, B. E.; Apponi, A. J. *Astrophys. J.* **2001**, *561*, L207.

(14) (a) Xu, X.; Pacey, P. *Phys. Chem. Chem. Phys.* **2005**, *7*, 326. (b) Calcote, H. F.; Keil, D. G. *Pure Appl. Chem.* **1990**, *62*, 815.

(15) Momoh, P. O.; Abrash, S. A.; Mabrouki, R.; El-Shall, M. S. *J. Am. Chem. Soc.* **2006**, *128*, 12408.

(16) Momoh, P. O.; El-Shall, M. S. *Chem. Phys. Lett.* **2007**, *436*, 25.

(17) Fairley, D. A.; Scott, G. B. I.; Freeman, C. G.; Maclagan, R.; McEwan, M. J. *J. Chem. Soc., Faraday Trans.* **1996**, *92*, 1305.

(18) Tzeli, D.; Mavridis, A.; Xantheas, S. S. *J. Chem. Phys.* **2000**, *112*, 6178.

(19) Tzeli, D.; Mavridis, A.; Xantheas, S. S. *Chem. Phys. Lett.* **2001**, *340*, 538.

(20) Tzeli, D.; Mavridis, A.; Xantheas, S. S. *J. Phys. Chem. A* **2002**, *106*, 11327.

(21) Dykstra, C. E. *J. Phys. Chem.* **1995**, *99*, 11680.

(22) van Voorhis, T.; Dykstra, C. E. *Mol. Phys.* **1996**, *87*, 931.

(23) Engdahl, A.; Nelander, B. *Chem. Phys. Lett.* **1983**, *100*, 129.

(24) Peterson, K. I.; Klemperer, W. *J. Chem. Phys.* **1984**, *81*, 3842.

(25) Silva, S. C.; Devlin, J. P. *J. Phys. Chem.* **1994**, *98*, 10847.

(26) Block, P. A.; Marshall, M. D.; Pedersen, L. G.; Miller, R. E. *J. Chem. Phys.* **1992**, *96*, 7321.

(27) Rusyniak, M.; Ibrahim, Y.; Alsharaeh, E.; Meot-Ner, M.; El-Shall, M. S. *J. Phys. Chem. A* **2003**, *107*, 7656.

(28) Rusyniak, M. J.; Ibrahim, Y. M.; Wright, D. L.; Khanna, S. N.; El-Shall, M. S. *J. Am. Chem. Soc.* **2003**, *125*, 12001.

(29) Curtiss, L. A.; Raghavachari, K.; Redfern, P. C.; Rassolov, V.; Pople, J. A. *J. Chem. Phys.* **1998**, *109*, 7764.

(30) Curtiss, L. A.; Redfern, P. C.; Raghavachari, K.; Rassolov, V.; Pople, J. A. *J. Chem. Phys.* **1999**, *110*, 4703.

(31) Frisch, M. J.; Trucks, G. W.; Schlegel, H. B.; Scuseria, G. E.; Robb, M. A.; Cheeseman, J. R.; Zakrzewski, V. G.; Montgomery, J. A.; Stratmann, R. E.; Burant, J. C.; Daprich, S.; Millam, J. M.; Daniels, A. D.; Kudin, K. N.; Strain, M. C.; Farkas, O.; Tomasi, J.; Barone, V.; Cossi, M.; Cammi, R.; Mennucci, B.; Pomelli, C.; Adamo, C.; Clifford, S.; Ochterski, J.; Petersson, G. A.; Ayala, P. Y.; Cui, Q.; Morokuma, K.; Malick, D. K.; Rabuck, A. D.; Raghavachari, K.; Foresman, J. B.; Cioslowski, J.; Ortiz, J. V.; Baboul, A. G.; Stefanov, B. B.; Liu, G.; Liashenko, P.; Piskorz, P.; Komaromi, I.; Gomperts, R.; Martin, R. L.; Fox, D. J.; Keith, T.; Al-Laham, M. A.; Peng, C. Y.; Nanayakkara, A.; Gonzalez, C.; Challacombe, M.; Gill, P. M. W.; Johnson, B. G.; Chen, W.; Wong, M. W.; Andres, J. L.; Gonzalez, C.; Head-Gordon, M.; Replogle, E. S.; Pople, J. A. *Gaussian 03*, revision C.02; Gaussian, Inc.: Pittsburgh, PA, 2004.

(32) Mason, E. A.; McDaniel, E. W. *Transport Properties of Ions in Gases*; Wiley & Sons: New York, 1988.

(33) Mesleh, M. F.; Hunter, J. M.; Shvartsburg, A. A.; Schatz, G. C.; Jarrold, M. F. *J. Phys. Chem.* **1996**, *100*, 16082.

(34) Morris, R. A.; Viggiano, A. A.; Paulson, J. F.; Henchman, M. J. *J. Am. Chem. Soc.* **1991**, *113*, 5932.

(35) Ibrahim, Y. M.; Mautner, M. N.; Alshraeh, E. H.; El-Shall, M. S.; Scheiner, S. *J. Am. Chem. Soc.* **2005**, *127*, 7053.

(36) *NIST Chemistry WebBook*; Linstrom, P. J., Mallard, W. G., Eds.; NIST Standard Reference Database Number 69; National Institute of Standards and Technology: Gaithersburg, MD, May 2007 (http://webbook.nist.gov).

(37) Mabud, M. A.; Ast, T.; Verma, S.; Jiang, Y. X.; Cooks, R. G. *J. Am. Chem. Soc.* **1987**, *109*, 7597.

(38) Ma, N. L.; Wong, M. W. *Eur. J. Org. Chem.* **2000**, 1411.

(39) Nobes, R. H.; Bouma, W. J.; Radom, L. *J. Am. Chem. Soc.* **1983**, *105*, 309.

(40) Terlouw, J. K.; Heerma, W.; Holmes, J. L. *Org. Mass Spectrom.* **1981**, *16*, 306.

(41) Mautner, M. N.; Elmore, D. E.; Scheiner, S. *J. Am. Chem. Soc.* **1999**, *121*, 7625.

(42) Mabrouki, R.; Ibrahim, Y.; Xie, E. L.; Mautner, M. M. N.; El-Shall, M. S. *J. Phys. Chem. A* **2006**, *110*, 7334.

(43) Meot-Ner, M. *Chem. Rev.* **2005**, *105*, 213.

(44) Davidson, W. R.; Lau, Y. K.; Kebarle, P. *Can. J. Chem.* **1978**, *56*, 1016.

JP802086Z